Available online at www.sciencedirect.com
SCIENCE DIRECT®
International Journal of Heat and Mass Transfer 48 (2005) 3648–3659
International Journal of HEAT and MASS TRANSFER
www.elsevier.com/locate/ijhmt

Application of the lattice Boltzmann method for solving the energy equation of a 2-D transient conduction–radiation problem

Subhash C. Mishra [a], Anjaneyulu Lankadasu [a], Kamen N. Beronov [b,*]

[a] Department of Mechanical Engineering, Indian Institute of Technology Guwahati, India
[b] Institute of Fluid Mechanics, University Erlangen, Nürnberg, Germany

Received 4 August 2004
Available online 26 May 2005

Abstract

A lattice Boltzmann method (LBM) is used to solve the energy equation in a test problem involving thermal radiation and to thus investigate the suitability of scalar diffusion LBM for a new class of problems. The problem chosen is transient conductive and radiative heat transfer in a 2-D rectangular enclosure filled with an optically absorbing, emitting and scattering medium. The energy equation of the problem is solved alternatively with a previously used finite volume method (FVM) and with the LBM, while the radiative transfer equation is solved in both cases using the collapsed dimension method. In a parametric study on the effects of the conduction–radiation parameter, extinction coefficient, scattering albedo, and enclosure aspect ratio, FVM and LBM are compared in each case. It is found that, for given level of accuracy, LBM converges in fewer iterations to the steady-state solution, independent of the influence of radiation. On the other hand, the computational cost per iteration is higher for LBM than for the FVM for a simple grid. For coupled radiation–diffusion, the LBM is faster than the FVM because the radiative transfer computation is more time-consuming than that of diffusion.

1. Introduction

Over the last 10 years, the lattice Boltzmann method (LBM) has evolved as an alternative numerical approach for the solution of a large class of problems [1–7]. Traditional CFD techniques solve the macroscopic transport equations of fluid flow, mass and heat transfer by directly discretizing them. Common numerical methods for solving the Navier–Stokes equations and the energy equation involve discretization of these nonlinear partial differential equations by finite difference methods (FDM), finite volume methods (FVM), etc. LBM use, on the other hand, kinetic equation models and corresponding relations between the actually simulated statistical dynamics at a microscopic level and the transport equations at the macroscopic level. This bottom–up approach of LBM assures by construction the conservation of the relevant macroscopic quantities such as mass and momentum [1]. LBM inherits many of the advantages of molecular dynamics and kinetic theories, due to its microscopic origin. But it does not use complicated kinetic equations. In comparison with the conventional CFD methods, the advantages of LBM include simple

* Corresponding author. Tel.: +49 9131 852 8280; fax: +49 9131 582 9503.
E-mail address: kberonov@lstm.uni-erlangen.de (K.N. Beronov).

0017-9310/$ - see front matter © 2005 Elsevier Ltd. All rights reserved.
doi:10.1016/j.ijheatmasstransfer.2004.10.041

Nomenclature

a	anisotropy factor
C	heat capacity
C_p	specific heat at constant pressure
c_j	weight factor in the CDM
c_v	information propagation velocity on the lattice
$f_{(i)}$	particle distribution density function in the ith direction
$f_{(i)}^{eq}$	equilibrium distribution density function in the ith direction
$w_{(i)}$	weight factor in the ith lattice direction
G	effective incident radiant energy
I	effective intensity of radiation
K	number of propagation directions in the lattice
k	thermal conductivity
M	total number of rays (intensities)
N	conduction–radiation parameter
Q_R	radiative heat flux
$\mathbf{r} = (x, y)$	2-D Cartesian coordinates
S	source function
s	geometric distance
T	temperature
t	time
Δt	time step
ΔX, ΔY	lengths of the enclosure in x- and y-directions lattice size in LBM or control volume size in FVM and CDM

Greek symbols

α	thermal diffusivity
β	extinction coefficient
θ	planar angle
κ_a	radiation absorption coefficient
η	collapsing coefficient
ε	emissivity
ρ	density
σ	Stefan–Boltzmann constant
σ_s	scattering coefficient
τ	relaxation time
ω	scattering albedo
$\boldsymbol{\xi}^{(i)}$	propagation vector in the ith lattice direction
ζ	non-dimensional time ($\alpha\beta^2 t$)

calculation procedure, simple and efficient implementation for parallel computation, easy and robust handling of complex geometries, and others [1–8]. The LBM is second-order accurate in time and space, which is sufficient for most engineering applications and, provided that boundaries are appropriately treated, makes LBM competitive for complex domain geometries.

Although the LBM has found wide usage in fluid mechanics [1,9] and its application to heat transfer problems is also gaining momentum [2,5–8,10–12], literature on its usage to solve heat transfer problems involving thermal radiation is scarce. Mishra and Lankadasu [13] applied a LBM to solve transient conduction and radiation heat transfer for the first time, for a case of a 1-D planar absorbing, emitting and scattering medium. They used the discrete transfer method to compute the radiative information. For that case, the LBM was found to provide accurate results but to be slower than the FDM/FVM, both with and without radiation. On the other hand, it has been established in hydrodynamic applications that LBM have computational advantages in multi-dimensional and complex geometries. LBM are thus viewed as a possible alternative to the FVM for computing the diffusive part of radiative–diffusive heat transfer in such geometries.

The objective of the present work is to compare the performance of the LBM in solving transient conduction and radiation heat transfer in a simple 2-D geometry against the performance of a standard CFD method. To that end, a benchmark problem [14–17] dealing with transient conduction and radiation heat transfer in a 2-D rectangular enclosure with absorbing, emitting and scattering media is considered. The LBM performance in solving the energy equation is compared against that of a FVM. The collapsed dimension method (CDM) is used to compute the radiative information [17,18] required as source in the energy equation, both in combination with the LBM and with the FVM. Results for the effects of the conduction–radiation parameter N, the scattering albedo ω, the extinction coefficient β, and the aspect ratio Y/X where X and Y are the dimensions of the 2-D enclosure, are studied.

The paper is organized as follows. Section 2 introduces the problem setting, including the relevant equations, boundary conditions, the studied parameter ranges, as well as discretization aspects such as the regular grid structure and resolution, the CDM approach to approximate the radiation equation, and the coupling between the diffusion and the radiation solver. The present article focuses on the LBM as diffusion solver, so a separate Section 3 is devoted to its detailed description. The results of the parametric study and the comparison are presented in Section 4. The article concludes with a brief discussion of these results.

2. Formulation

The heat transfer in a 2-D rectangular enclosure heated from below by sustaining the temperature of its alls at time-independent but different temperatures is considered. The naming of coordinate directions and of enclosure walls is given in Fig. 1. With these, the initial condition at time $t = 0$ for the temperature field $T(x, y, t)$ is given by a constant T_0:

$$T(x, y, 0) = T_0 \tag{1}$$

and the boundary conditions at $t > 0$ by

$$T(0, y, t) = T_0, \quad T(X, y, t) = T_0, \tag{2a}$$

$$T(x, 0, t) = T_S, \quad T(x, Y, t) = T_0, \tag{2b}$$

where T_S is another constant. This set of conditions is formally inconsistent, because $T(0, 0, t)$ and $T(X, 0, t)$ are not uniquely defined. The mathematical solution to the corresponding heat equation,

$$\frac{\partial T}{\partial t} = \alpha \nabla^2 T + \frac{Q_R}{C}, \qquad C = \rho C_R, \tag{3}$$

has thus singularities confined to the lower edges of the enclosure. Such problems are often encountered in the engineering practice, despite their mathematical difficulty and possible numerical instability, depending on the method used. FVM work with integrated quantities and can deal with the singularity without special effort. It is of interest here to verify the robustness of LBM, which is formally dealing only with point-values, in such situations.

In Eq. (3) the thermophysical properties of the medium, such as the density ρ, the specific heat C_p and heat capacity C, and the thermal diffusivity α are assumed to be constant. From a radiative energy transfer point of view, the walls of the enclosure are considered to be diffuse and gray, and the contained medium to be gray, absorbing and emitting, anisotropically scattering, and homogeneous. The optical properties of the radiating medium are the

- scattering coefficient σ_s,
- absorption coefficient κ_a,
- extinction coefficient $\beta = \kappa_a + \sigma_s$,
- scattering albedo $\omega = \sigma_s/\beta$.

And are also assumed to be constant.

The energy equation (3) can be solved by standard methods such as FDM or FVM, but also by LBM. The radiative source Q_R in it can be provided by for solving the radiative transfer equation (RTE), which reads

$$\frac{\mathrm{d}}{\mathrm{d}} I(s, \xi) = -\beta I(s, \xi) + \kappa_a \frac{\sigma T^4}{4\pi} + \frac{\sigma_s}{4\pi} \oint_{|\xi'|=1} \Phi(\xi, \xi') I(s, \xi') \, \mathrm{d}\xi' \tag{4}$$

in general. An approximate numerical solution of the RTE can be obtained by any of the commonly used methods, such as the discrete ordinate method, the discrete transfer method, the finite volume method (FVM), or the collapsed dimension method (CDM). In this study, only the CDM is used to compute Q_R. This method introduces a specific 2-D approximation for the RTE.

2.1. Collapsed dimension method

In the CDM, the radiative source is given by [18]

$$Q_R = \eta \kappa_a (G - \pi \sigma T^4), \tag{5}$$

where η is the collapsing coefficient, κ_a is the absorption coefficient and G is the effective incident radiation, whose general form and CDM approximation [18] are given by

$$G = \int_0^{2\pi} I(\theta) \, \mathrm{d}\theta \approx \sum_{j=1}^{M} I(\theta_j) \Delta\theta_j, \tag{6}$$

where θ is the angle of the effective intensity I measured from the control surface. The effective intensity at any location in direction θ in the solution plane is found from the recursive use of the following equation:

$$I_{n+1} = (1 - \lambda) I_n + \lambda S_n, \quad \lambda = 1 - \exp(-\eta\beta\Delta s). \tag{7}$$

The basis for the approximate method (7) is the assumption that the optical path-leg $\beta\Delta s$ between the downstream point $(n + 1)$ and the upstream point n is small enough and the source function S (given by Eq. (8) below) is constant over this optical path-leg. For the

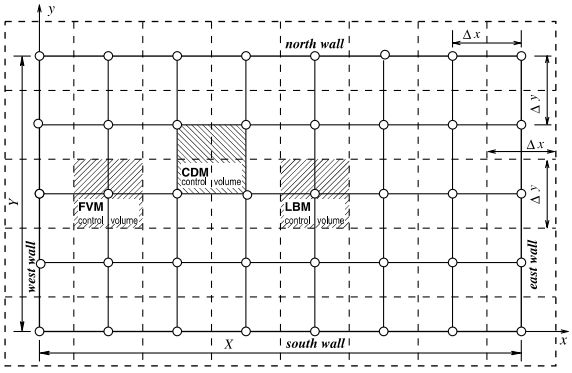

Fig. 1. Geometry and the coordinates of the problem under consideration. Nomenclature of the lattice in the LBM and the control volume used in the CDM are also shown. Centres of the lattices are the corners of the control volume where radiative information are computed in the CDM.

case of a linear anisotropic phase function Φ with anisotropy factor a, the source function S is given in the CDM [18] in terms of G and Q_R as

$$S = \kappa_a \frac{\sigma T^4}{2} + \frac{\sigma_s}{2\pi}(G + aQ_R \sin\theta). \tag{8}$$

The net radiative heat flux Q_R is numerically evaluated [18] in the CDM as

$$\begin{aligned} Q_R &= \int_0^{\pi} I(\theta)\sin\theta\,d\theta - \int_{\pi}^{2\pi} I(\theta)\sin\theta\,d\theta \\ &\approx \sum_{j=1}^{M/2} c_j I(\theta_j) - \sum_{j=M/2+1}^{M} c_j I(\theta_j), \end{aligned} \tag{9}$$

where the weight factor c_j is chosen as

$$c_j = |\cos(\theta_j + \Delta\theta_j/2) - \cos(\theta_j - \Delta\theta_j/2)|. \tag{10}$$

In Eqs. (6) and (9), M is the number of effective intensities spanned over $0 \leqslant \theta \leqslant 2\pi$, and $\Delta\theta_j$ is the discrete angle in the 2-D plane over which the jth effective intensity is assumed to be isotropic. In the present case, $\Delta\theta_j$ is same for all effective intensities.

For a diffuse–gray boundary with temperature T_0 and emissivity ε_b, the boundary data I_0 for I are calculated in the CDM as follows:

$$\begin{aligned} I_0 &= T_0^4\varepsilon_b/2 + J(I_0)(1-\varepsilon_b)/2, \\ J(I) &= \int_0^{\pi} I(\theta)\,d\theta \approx \sum_{j=1}^{M/2} c_j I(\theta_j). \end{aligned} \tag{11}$$

The CDM has been verified for a variety of test problems, including ones related to the one considered here, but not in conjunction with LBM. More details on the CDM can be found in [17,18].

2.2. Test problem

For the present validation purpose, only isotropic scattering ($a = 0$) was considered. Throughout the simulations, the south wall is kept at a constant temperature T_S, allowing the introduction of the conduction–radiation parameter N as a constant characterizing a given computation:

$$T_S = 2T_0, \quad N = k\beta/4\sigma T_S^3. \tag{12}$$

Radiative information was computed using 32 rays in the CDM. Uniform meshes of 20×20 control volumes (CVs) were used in both FVM and LBM, which was found sufficient for grid-independent results. The same number of CVs was used in the CDM. (For the relation between the different types of CVs see Fig. 1.) To solve Eq. (3) by the FVM, the alternating direction implicit scheme was employed. Both LBM and FVM were applied as transient solvers with non-dimensional time step of fixed, sufficiently small length:

$$\Delta\zeta = 10^{-4}, \quad \zeta = \alpha\beta^2 t.$$

The steady-state (SS) was assumed to be reached if the relative point-wise temperature difference between two consecutive time steps (at each lattice node in the LBM or control volume centre in the FVM) did not exceed 10^{-5}.

The LBM and the FVM results, obtained in conjunction with the CDM, were first validated against those available in the literature [14–17]. Results at different time levels, obtained by coupling FVM with the CDM as RTE solver, were further benchmarked again results obtained by coupling FVM with the discrete transfer method instead.

3. Lattice Boltzmann method

Although the discretized equation solved in LBM is rather different from any other standard method for simulating heat and mass flow, it is in effect only one further option to approximate numerically the diffusion-advection equations governing the computed flow. In the present case, this is the heat flow equation

$$(\partial/\partial t + \mathbf{v}\cdot\nabla)T = \alpha\nabla^2 T + Q$$

for the special case of no advection ($\mathbf{v} = 0$) and a source Q defined entirely by radiation. A detailed demonstration that the discrete evolution equation solved in the LBM indeed approximates the above scalar flow equation is provided in Appendix A, while the computational algorithm of the LBM is given immediately below. It may appear unusual that, unlike standard methods which are derived starting from the flow equation and then applying various discretizations, in the LBM approach the approximation to the flow equation is only shown after the method is already postulated. On the other hand, standard discretization methods require such an a posteriori proof that they indeed approximate the target equation. Also, different discretization methods have very different numerical properties and usually have their specific jargon and notation. Thus, LBM should be considered only as one of several alternatives for solving the target flow equation. The selection of a particular alternative for actual simulations is then dictated not by theoretical, but by practical issues such as robustness or speed. And LBM can have advantages in such aspects while delivering a degree of approximation comparable to most other, customary methods.

3.1. Kinetic equation

The formal starting point for the analysis of any LBM [1–4] is a discrete velocity model for a kinetic equation, with collision kernel $\Omega(f)$, describing the evolution of a distribution density function f of a scalar field

such as the material density ρ of a continuum. In the present case, the scalar field of interest is the temperature $T(\mathbf{r},t)$.

The basis of the discrete velocity model is a finite set of virtual velocities $\boldsymbol{\xi}^{(i)}$ or equivalently, of virtual fluxes of the considered scalar field, say T. To each such velocity or flux, a probability $f_{(i)}$ is associated, individually for each location and time $(\mathbf{r},t)$, in such a way that the scalar field at that point is

$$T(\mathbf{r},t)=\sum_i f_{(i)}(\mathbf{r},t)$$

and its observed flux is $\sum_i f_{(i)}(\mathbf{r},t)\boldsymbol{\xi}^{(i)}$.

The virtual velocities $\boldsymbol{\xi}^{(i)}$ constitute a lattice stencil characterizing the particular lattice Boltzmann model. The well-known D2Q9 lattice model (Fig. 2) will be considered here. In that model, the set of $\boldsymbol{\xi}^{(i)}$'s is such that they connect the point, on which the lattice stencil is centred, to its nearest neighbours on a spatial grid with uniform spacing in both coordinate directions (a lattice).

Any LBM advances the probability densities $f_{(i)}(\mathbf{r},t)$ in time and thereby computes the evolution of the considered scalar. In the absence of external sources or fluxes for the scalar, the corresponding discrete evolution equation can be written in the following general form:

$$(\partial/\partial t+\boldsymbol{\xi}^{(i)}\cdot\nabla)f_{(i)}(\mathbf{r},t)=\Omega_i,\quad i=0,1,2,\ldots,K. \tag{13}$$

The collision term Ω_i incorporates all the physics and modeling of any particular problem at hand. The simplest model for Ω_i is the Bhatnagar–Gross–Krook (BGK) model [19]

$$\Omega_i=(f^{\mathrm{eq}}_{(i)}-f_{(i)})/\tau. \tag{14}$$

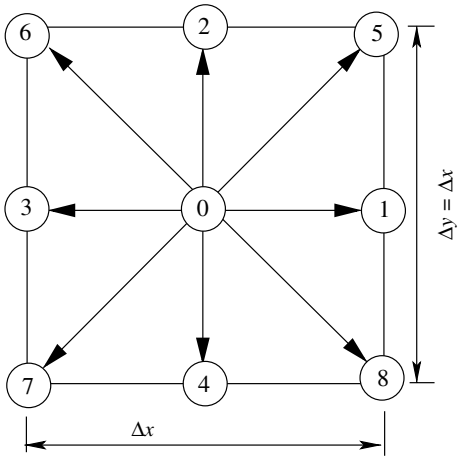

Fig. 2. Schematic diagram of the D2Q9 lattice. The directions of the eight non-zero propagation vectors $\boldsymbol{\xi}^{(1)}$ through $\boldsymbol{\xi}^{(8)}$ are shown.

It is a single-relaxation-time model with relaxation constant τ that can be related, via Chapmann–Enskog analysis, to the diffusivity (viscosity) of the medium. In original BGK model, the equilibrium distribution density function is prescribed as Maxwellian. In all corresponding lattice models, the discrete equilibrium density distributions $f^{\mathrm{eq}}_{(i)}$ are derived from that Maxwellian distribution through an approximation consistent with the approximation of the continuous f by the discrete set of $f_{(i)}$'s.

3.2. Lattice model

When convection can be neglected, the Maxwellian-like equilibria are not shifted and a modified Chapmann–Enskog analysis with only one time scale is relevant. The convective time scale is omitted and the slower, diffusive scale is left [4]. The analysis then shows (cf. also Appendix A) that the zero-order moment $M_0[\cdot]=\sum_{i=0}^{K}(\cdot)$, when applied to Eq. (13) with the BGK term (14) substituted into the right-hand side, gives a diffusion equation for the evolution of the scalar, with a diffusivity proportional to τ. The scalar itself is obtained by applying M_0 to the distribution density.

The above considerations are general. For the D2Q9 model in particular,

$$\boldsymbol{\xi}^{(0)}=(0,0), \tag{15a}$$

$$\boldsymbol{\xi}^{(1)}=(c_{\mathrm{v}},0),\qquad \boldsymbol{\xi}^{(2)}=(0,c_{\mathrm{v}}), \tag{15b}$$

$$\boldsymbol{\xi}^{(3)}=(-c_{\mathrm{v}},0),\qquad \boldsymbol{\xi}^{(4)}=(0,-c_{\mathrm{v}}), \tag{15c}$$

$$\boldsymbol{\xi}^{(5)}=(c_{\mathrm{v}},c_{\mathrm{v}}),\qquad \boldsymbol{\xi}^{(6)}=(-c_{\mathrm{v}},c_{\mathrm{v}}), \tag{15d}$$

$$\boldsymbol{\xi}^{(7)}=(-c_{\mathrm{v}},-c_{\mathrm{v}}),\qquad \boldsymbol{\xi}^{(8)}=(c_{\mathrm{v}},-c_{\mathrm{v}}). \tag{15e}$$

The equilibrium distributions are obtained from the leading-order moments of the $f_{(i)}$'s. In the present case, there is no convection, so the first-order moment vanishes, while the zero-order moment gives the temperature, which is the scalar of interest here. This interpretation of temperature as an independent scalar is clearly distinct from that in the so-called thermal LBM. In the present case and with the chosen model,

$$T(\mathbf{r},t)=\sum_{i=0}^{K}f_{(i)}(\mathbf{r},t)=\sum_{i=0}^{K}f^{\mathrm{eq}}_{(i)}(\mathbf{r},t),$$
$$f^{\mathrm{eq}}_{(i)}(\mathbf{r},t)=w_{(i)}T(\mathbf{r},t), \tag{16}$$

$$w_{(0)}=4/9,\quad w_{(i)}=1/9,\ \ i=1,\ldots,4,$$
$$w_{(i)}=1/36,\ \ i=5,\ldots,8. \tag{17}$$

The following constraint imposed on lattice models may be noted:

$$\sum_{i=0}^{K}w_{(i)}=1\Longleftrightarrow\sum_{i=0}^{K}f_{(i)}=\sum_{i=0}^{K}f^{\mathrm{eq}}_{(i)}, \tag{18a}$$

$$\sum_{i=0}^{K}w_{(i)}\boldsymbol{\xi}^{(i)}=\mathbf{0}\Longleftrightarrow\sum_{i=0}^{K}\boldsymbol{\xi}^{(i)}f_{(i)}=\sum_{i=0}^{K}\boldsymbol{\xi}^{(i)}f^{\mathrm{eq}}_{(i)}. \tag{18b}$$

3.3. The forced lattice Boltzmann equation

To represent the source term of the heat equation (3), an additional term $q_{(i)}$ must be added to the right-hand side of the kinetic equation (13), such that when M_0 is applied to it, the source term Q_R/C will result. This can be done by emulating the construction of $f^{eq}_{(i)}$ in Eq. (16):

$$(\partial/\partial t + \boldsymbol{\xi}^{(i)} \cdot \nabla) f_{(i)}(\mathbf{r}, t) = (f^{eq}_{(i)} - f_{(i)})/\tau + q_{(i)}, \tag{19}$$

$$q_{(i)} = -w_{(i)} Q_R / C. \tag{20}$$

It is then standard for LBM to discretize the first-order derivatives on the left-hand side of Eq. (19) by forward first-order finite differences:

$$\frac{\partial}{\partial t} f_{(i)}(\mathbf{r}, t) = \frac{f_{(i)}(\mathbf{r}, t + \Delta t) - f_{(i)}(\mathbf{r}, t)}{\Delta t} + O(\Delta t),$$

$$\boldsymbol{\xi}_{(i)} \cdot \nabla f_{(i)}(\mathbf{r}, t) = \frac{f_{(i)}(\mathbf{r} + \boldsymbol{\xi}_{(i)} \Delta t, t + \Delta t) - f_{(i)}(\mathbf{r}, t + \Delta t)}{c_v \Delta t} + O(\Delta t).$$

The resulting fully discretized equation then reads

$$f_{(i)}(\mathbf{r} + \boldsymbol{\xi}^{(i)} \Delta t, t + \Delta t) = f_{(i)}(\mathbf{r}, t) + (f^{eq}_{(i)}(\mathbf{r}, t) - f_{(i)}(\mathbf{r}, t)) \Delta t/\tau - \Delta t w_{(i)} Q_R / C. \tag{21}$$

The relaxation time can be related with the thermal diffusivity, the lattice velocity c_v and the time step [2,4] by the (approximate but practically precise) relation

$$\tau = 3\alpha/c_v + \Delta t/2. \tag{22}$$

This relation, as well as the derivation of the heat equation (3) from the kinetic equation (21), result from a Chapmann–Enskog type of expansion mentioned above and included for completeness of the article in Appendix A.

3.4. Implementation of boundary conditions

In the present study, the energy equation is subjected to Dirichlet boundary conditions. To assure that the prescribed temperature values are exactly imposed, the numerical grid is so constructed, that those grid points updated by the LBM, which are closest to the domain boundary in fact lie on it. For each of these points, there is only one datum, namely the temperature value. (The corner point issue has been discussed earlier. Here it suffices to say that at the south–east and south–west edges of the enclosure the value T_S and not T_0 was imposed.) But there are at least three (for the D2Q9 model) lattice directions, whose corresponding distribution density functions are unknown. Fixing the number density on the boundary [6,7,10,12] is required to impose the Dirichlet condition for a scalar whose dynamics is simulated with a LBM. From known boundary scalar density and (in our case zero) velocity at the boundary, the equilibrium distribution densities along all discrete directions can be computed, cf. (20). For the non-equilibrium part of those distribution densities, which correspond to directions entering the computational domain, however, assumptions have to be made. Most of the literature on this aspect of LBM adopts some variant of the so-called bounce-back rule for these densities: the incoming non-equilibrium parts equal their outgoing counterparts along the discrete direction exactly opposite to their own.

It is recalled that the non-equilibrium parts $f_{(i)} - f^{eq}_{(i)}$ carry the information about gradients of scalar flux. When the scalar is mass density of a fluid moving with velocity $\mathbf{v}(\mathbf{r}, t)$, their second moment gives the stress tensor which is proportional, as found by a Chapman–Enskog analysis, to the strain tensor $(\nabla\mathbf{v} + (\nabla\mathbf{v})^T)/2$. In the present case, their second moment is related to $\nabla\nabla T$ (cf. Appendix A).

If the field $T(\mathbf{r}, t)$ *were* stationary, and if there *were* to be no scalar source, then $\nabla^2 T = 0$ *would* hold and the assumption of $\nabla\nabla T = \mathbf{0}$ *would* be a plausible approximation. It would in turn imply, if invariance with respect to the discrete rotation group associated with the lattice directions is required, a detailed balance of fluxes in opposite directions, such as

$$(f^{eq}_{(1)}(0, y, t) - f_{(1)}(0, y, t)) + (f^{eq}_{(3)}(0, y, t) - f_{(3)}(0, y, t)) = 0 \tag{23}$$

for a point on the west wall. In the present case, the walls of the enclosure are kept at constant temperature, so thermal equilibrium in the walls and thus absence of thermal source exactly on the boundary can be assumed. Moreover, the purpose of the computation is the achievement of a steady-state. On these grounds, the detailed cancellation described above will be assumed and used to specify the boundary conditions.

The above (anti)symmetry relation of corresponding non-equilibrium pairs is an instantaneous equality and not, as in the usual bounce-back rule which assumes that the domain boundary is half-way between neighbouring lattice sites, an equality with phase shift of one time step. It leads to a unique rule for treating the Dirichlet boundary conditions, which will now be illustrated on the example of a lattice grid point $(0, y)$ lying on the west boundary. The three unknown incoming particle distribution density functions are $f_{(1)}$, $f_{(5)}$, and $f_{(8)}$ (cf. Fig. 2). In view of Eq. (16), one has e.g.

$$f^{eq}_{(1)}(0, y, t) = f^{eq}_{(3)}(0, y, t) = w_{(1)} T(0, y, t) = T_0/9 \tag{24}$$

for all times $t \geqslant 0$. Thus, using the flux balance (23), the unknown density function

$$f_{(1)}(0,y,t) = f^{eq}_{(1)}(0,y,t) - f_{(3)}(0,y,t) + f^{eq}_{(3)}(0,y,t) = (2/9)T_0 - f_{(3)}(0,y,t). \quad (25)$$

All other cases of lattice directions and wall locations are treated similarly, cf. Appendix B.

3.5. Solution procedure

It is now possible to formulate the LBM simulation procedure in full. The numerical grids, the initialization procedure and the time stepping procedure are specified in order.

The medium is divided into a finite number of control volumes. The nodes of the control volume faces at which the radiative information is computed in the CDM are the centres of the lattices in the LBM (Fig. 1). To satisfy the boundary conditions, the LBM grid points are taken to lie precisely on the boundary. Thus, the LBM control volumes along the boundary extend beyond the boundaries a distance equal to half the lattice size in the respective coordinate directions (Fig. 1).

The LBM initialization procedure for the energy equation follows:

1. Calculate the relaxation time τ from Eq. (22).
2. Given the initial temperature field, compute $f^{eq}_{(i)}(\mathbf{r}, t = 0)$ from Eq. (16) and then set $f_{(i)}(\mathbf{r}, 0) = f^{eq}_{(i)}(\mathbf{r}, 0)$.

The procedure for solving the energy equation using the LBM is to repeat at every time step the following sequence:

1. With the temperature field known, calculate the heat source Q_R using the CDM.
2. Calculate now the particle distribution functions $f_{(i)}(\mathbf{r} + \boldsymbol{\xi}\Delta t,\ t + \Delta t)$ using Eq. (21).
3. Propagate the particle distribution functions to the neighbouring nodes.
4. Calculate the new temperature field $T(\mathbf{r}, t)$ using Eq. (16).
5. Check for convergence and terminate the cycle, if appropriate.
6. Modify the particle distribution functions locally, to satisfy the boundary conditions.
7. Compute the equilibrium distribution function $f^{eq}_{(i)}(\mathbf{r}, t)$ from the new temperature field, using Eq. (16), separately for every lattice node.

4. Results and discussion

We investigate first the effect of LBM grid size on non-dimensional temperature T/T_S by comparing the steady-state (SS) results at three locations along the centreline $x/X = 0.5$ of the enclosure. Results obtained for aspect ratio $X/Y = 1$, extinction coefficient $\beta = 1$, scattering albedo $\omega = 0.5$, and conduction–radiation parameter $N = 0.1$, are listed in Table 1. It is seen that on grids 20×20 and larger, the maximum variation in temperature is less than 5×10^{-4}. The trend observed with other sets of parameters was similar, and need not be reproduced here. It was decided to use 20×20 grids as basis for the subsequent computations. To facilitate the comparison of results, all further reported data were taken only at $x/X = 0.5$. They represent the normalized temperature T/T_S as function of the normalized distance y/Y to the "south" wall, which is kept at temperature T_S.

These results are summarized in Figs. 3–6. The effect of the conduction–radiation parameter N is demonstrated in Fig. 3 (see also Fig. 4b). The effect of the extinction coefficient β is shown in Fig. 4, and that of the scattering albedo ω in Fig. 5. The results in these figures are obtained for $X/Y = 1$. The effect of the aspect ratio is illustrated in Fig. 6, where the presented data are obtained for $X/Y = 10$ and are close to those for a 1-D planar medium.

A radiation-dominated solution ($N = 0.01$, Fig. 3a) can be compared to a conduction-dominated solution ($N = 1$, Fig. 3b) for an absorbing–emitting medium (no scattering, $\omega = 0$) in Fig. 3. The SS results by the LBM and the FVM compare very well. It can also be seen that at certain times there is mismatch in the transient results of the two methods, whereby the LBM results are slightly closer to the SS. This in agreement with a general observation (Table 2) that the LBM converges faster than the FVM to a SS. Finally, it is observed that the difference in the SS results by the two methods is more significant in the conduction-dominated case. This may be related to a lager difference in the number of iterations (Table 2) needed by the two methods in that case.

The effect of the extinction coefficient β is shown, again for an absorbing–emitting isotropic ($\omega = 0$) medium with $N = 0.1$, in Fig. 4. Two values of the extinction coefficient are compared: $\beta = 0.1$ (weakly participating medium, Fig. 4a) and $\beta = 1$ (strongly participating, Fig. 4b). The steady-state LBM and the FVM results are in a very good agreement. The LBM reaches SS faster.

Table 1
Effect of grid size in the LBM on non-dimensional temperature at three locations along the centreline $x/X = 0.5$

Resolution	$y/Y = 0.25$	$y/Y = 0.5$	$y/Y = 0.75$
8×8	0.7792	0.6453	0.5647
12×12	0.7815	0.6464	0.5648
16×16	0.7817	0.6469	0.5653
20×20	0.7820	0.6470	0.5654
40×40	0.7821	0.6473	0.5656

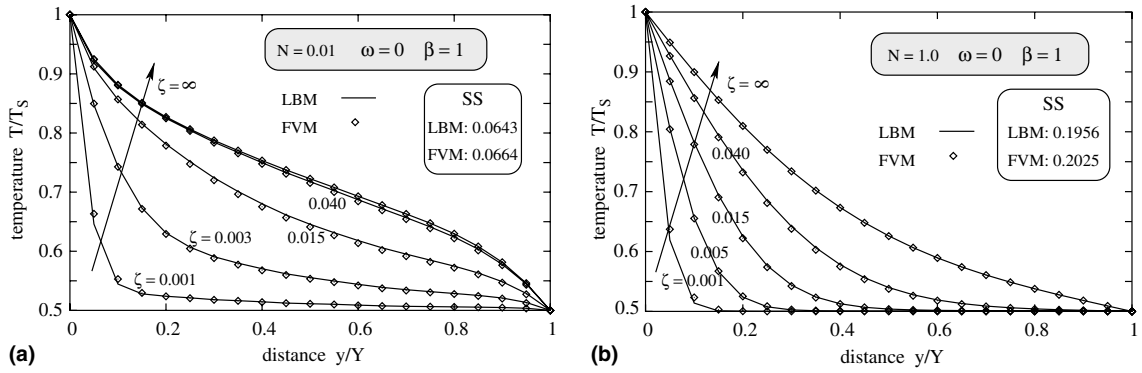

Fig. 3. Centerline temperature T/T_S at different non-dimensional times ζ for two values of the conduction–radiation parameter: (a) $N = 0.01$ and (b) $N = 1$.

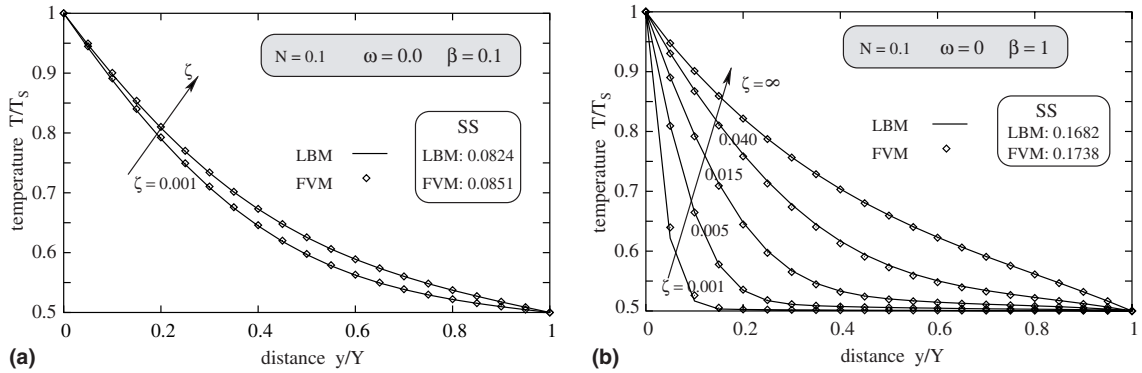

Fig. 4. Centerline temperature T/T_S at different non-dimensional times ζ for two values of the extinction coefficient: (a) $\beta = 0.1$ and (b) $\beta = 1$.

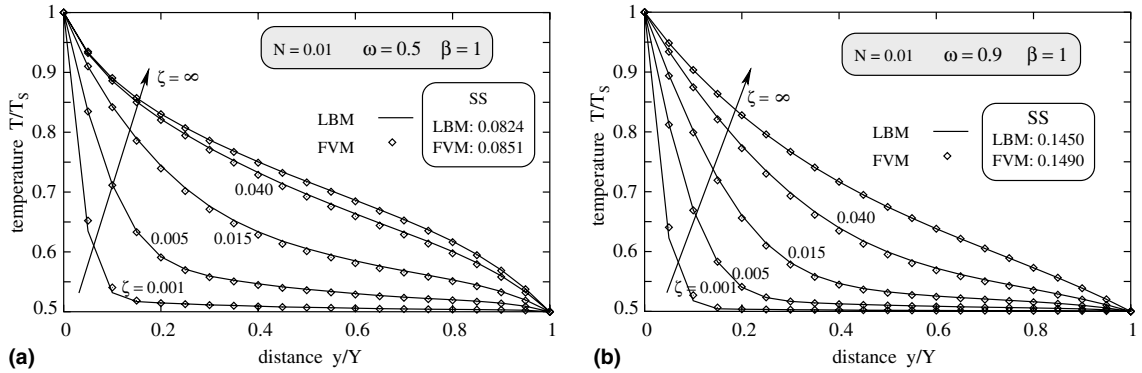

Fig. 5. Centerline temperature T/T_S at different non-dimensional times ζ for two values of the scattering albedo: (a) $\omega = 0.5$ and (b) $\omega = 0.9$.

The effect of scattering is similarly presented in Fig. 5, for fixed $N = 0.01$ and $\beta = 1$. The scattering albedo is set to nonzero values: $\omega = 0.5$ (scattering comparable to absorption, Fig. 5a) and $\omega = 0.9$ (strong scattering,

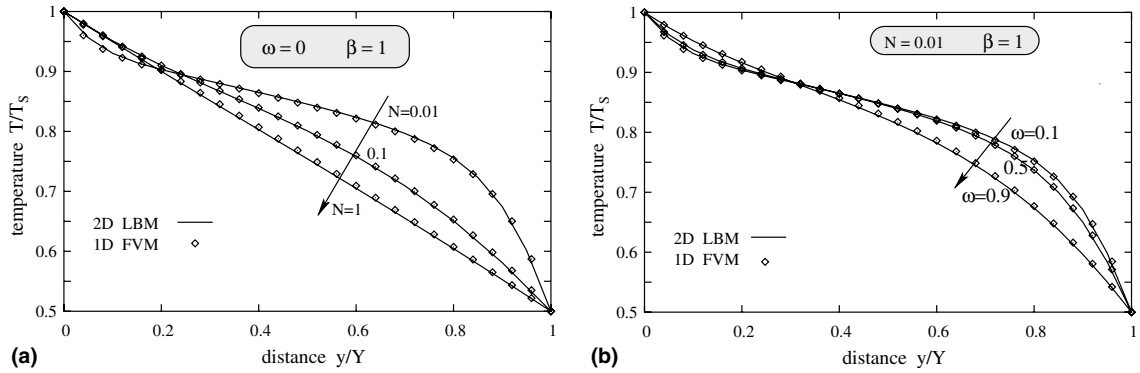

Fig. 6. Comparison of steady-state 2-D LBM and 1-D FVM results for the centreline temperature T/T_S at aspect ratio $X/Y = 10$.

Table 2
Comparison of the number of iterations required to obtain steady-state solutions with the LBM and the FVM, and of the corresponding CPU times ratio LBM/FVM, for 20×20 (40×40) control volumes

N	ω	LBM	FVM	FVM/LBM	Figure
0.01	0	642 (644)	663 (729)	1.05 (1.09)	3a
0.01	0.5	823 (825)	850 (930)	1.04 (1.10)	5a
0.01	0.9	1449 (1454)	1498 (1631)	1.03 (1.12)	5b
0.1	0	1682 (1689)	1738 (1895)	1.08 (1.10)	4b
1	0	1894 (1968)	2024 (2202)	1.07 (1.12)	3b

The same computer and the same CDM code with $\beta = 1$ was used to compute radiative information with both heat equation solvers.

Fig. 5b). With scattering, too, the SS obtained by the LBM and the FVM agree very well and the LBM is faster to reach it.

The effect of aspect ratio is illustrated in Fig. 6. In order to present it along with the effect of N or ω, only SS solutions are plotted. (The trend in the transient evolution, established in the previous figures, is discussed below.) The LBM results shown in this figure are for an aspect ratio $X/Y = 10$, large enough to approximate in the center of the enclosure with respect to the x-coordinate the temperature distribution in a 1-D slab geometry. To verify this expectation, these 2-D LBM simulation data are compared to predictions by a 1-D FVM–CDM code. Since the LBM grid cells must be squares, the one used here was 20:20, while the 1-D grid for the FVM had 100 cells. The non-scattering ($\omega = 0$) media appearing in Figs. 3 and 4b are compared in Fig. 6a. The scattering media from Fig. 5 ($N = 0.01$) are compared, along with a weakly scattering one ($\omega = 0.1$) in Fig. 6b. Although a slight finite-aspect-ratio effect can be discerned, the observed agreement between the 2-D LBM and the 1-D FVM results is very good.

It was observed that, as seen in Figs. 3–5, the LBM converges to the SS solution of the heat equation (3) faster, in terms of iteration number, than the FVM. To substantiate this quantitatively, data on the number of iterations and the relative CPU times required to compute the data in the mentioned figures are presented in Table 2. Also given (cited in brackets) are corresponding data for a 40×40 grid, to illustrate the effect of doubling the resolution on the two methods compared. The LBM is faster, due to a slightly lower number of iterations required for convergence. This advantage is more pronounced on the larger grid.

Let it be mentioned for reference, that when solving the transient 2-D conductive heat equation (3) without radiation ($Q_R = 0$) but with the same initial and boundary conditions for T as before, the relation between the two methods is somewhat different: The number of iterations was still smaller with the LBM than with the FVM (respectively 3056 and 3653) but the CPU time required by the LBM was about four times that of the FVM. It is the radiation transfer computation, which is very expensive even when using the presently fastest methods like CDM in 2-D, that turns the LBM into the method of choice because of its faster convergence in terms of number of iteration steps. Its advantage would become significant on larger grids.

5. Conclusions

A simple lattice Boltzmann method (LBM) was introduced as solver for the energy equation in 2-D transient conduction and radiation heat transfer problems. Its performance was studied on the example of isotropic gray

radiation in a rectangular enclosure with constant physical properties, by comparing it to a finite volume method (FVM). With both methods, the collapsed dimension method (CDM) was used to compute the radiative source term in the energy equation. The effects of various properties of the enclosure (its aspect ratio, the conduction–radiation parameter, the extinction coefficient, and the scattering albedo of the gray medium in it) were illustrated by a parametric study. Comparison of the data obtained in that study by both solvers, based on LBM and on FVM, showed very good agreement in the steady-state results. The LBM was found to be accurate and to require slightly fewer steps to converge to a steady-state.

The considered 2-D geometry was a simple one, to allow simple validation. Advection and other heat sources, such as combustion, were omitted. Thus, it remains to demonstrate the viability of the LBM as heat diffusion-advection solver and its robustness in the presence of considerable advection as well as of additional heat sources, especially localized ones. The results presented here and the efficacy and robustness of LBM in complex flows, known from the literature, allow the expectation that LBM may have advantages over conventional energy equation solvers, especially if the geometry or the physics of the problem is complex.

The results were obtained with very small grids, starting at 20×20 control volumes. This was found sufficient for the present purpose of verification and comparison. With increasing complexity, the grid size of future applications will increase. The presented results imply that the advantage of the LBM will then be more pronounced. Moreover, for very large problems the use of LBM will bring additional advantages on parallel computing platforms.

Acknowledgement

The first author thanks Prof. Franz Durst, Institute of Fluid Mechanics, Friedrich-Alexander University Erlangen-Nürnberg, for the motivation to explore LBM for thermal radiation problems.

Appendix A

The starting point of the analysis is an assumption of sufficient numerical resolution, in the form of a small parameter $0 < \varepsilon = \Delta y/Y \ll 1$, in which $\Delta x = \Delta y = \xi \Delta t$ is the LBM grid step size and Y is a length scale characterizing the spatial structure of the solution of Eq. (3). In the present article, the test problem of heat transfer in a rectangular enclosure with dimensions $X \geqslant Y$ is considered, and it was found empirically that taking $\Delta y = Y/20$, i.e. $\varepsilon = 0.05$, provides sufficient precision.

It is well known from standard numerical analysis of parabolic differential equations that, as the spatial grid step Δx of a solution algorithm for the standard heat transfer equation is decreased, the time step of an explicit time-marching scheme must decrease like $\Delta t = \mathrm{O}(\Delta x^2)$ in order to assure numerical stability. All LBM are based on explicit time stepping. When applied as heat equation solvers, their resolution must scale accordingly [4]:

$$\Delta x = \Delta y = \varepsilon Y, \quad \Delta t = \varepsilon^2 t_c, \tag{A.1}$$

$$\partial/\partial x = \varepsilon \partial'_x, \quad \partial/\partial t = \varepsilon^2 \partial'_t, \tag{A.2}$$

where t_c is a characteristic time scale, $t_c \sim C$ with C defined in Eq. (3). Then introduce

$$\partial_{(i)} = \boldsymbol{\xi}^{(i)} \cdot \nabla, \quad \partial'_{(i)} = \xi_x^{(i)} \partial'_x + \xi_y^{(i)} \partial'_y. \tag{A.3}$$

At this point, the assumption that all $f_{(i)}$'s are close to their respective $f_{(i)}^{\mathrm{eq}}$'s will be recalled. This has been the sole justification for introducing the BGK model in the first place. Here, it will be interpreted as implying that

$$f_{(i)} = f_{(i)}^{\mathrm{eq}} + f'_{(i)}\varepsilon + \mathrm{O}(\varepsilon)^2, \quad q_{(i)} = \varepsilon q'_{(i)},$$
$$f_{(i)}^{\mathrm{eq}}, f'_{(i)}, q'_{(i)} = \mathrm{O}(1) \Rightarrow f'_{(i)} = (q'_{(i)} - \partial'_{(i)} f_{(i)}^{\mathrm{eq}})\tau. \tag{A.4}$$

It is further noted that, using Eq. (18b) and a similar relation for second moments, one can show that

$$M_1[f^{\mathrm{eq}}] = \sum_{i=0}^{K} \boldsymbol{\xi}^{(i)} f_{(i)}^{\mathrm{eq}} = 0,$$
$$M_2[f^{\mathrm{eq}}] = \sum_{i=0}^{K} \boldsymbol{\xi}^{(i)} \otimes \boldsymbol{\xi}^{(i)} f_{(i)}^{\mathrm{eq}} = (c_v/3)\boldsymbol{I}, \tag{A.5}$$

where $\boldsymbol{I}$ denotes the identity operator and the factor 1/3 is specific to the lattice model used, namely D2Q9. Since $M_1[q'] = (Q_R/C)M_1[f^{\mathrm{eq}}] = 0$ in view of (A.5), the decomposition (A.4) implies also

$$M_1[f'] = \sum_{i=0}^{K} \boldsymbol{\xi}^{(i)} f'_{(i)} = 0. \tag{A.6}$$

Expanding the left-hand side function in Eq. (21),

$$\begin{aligned} f_{(i)}(\mathbf{r} + \boldsymbol{\xi}^{(i)}\Delta t, t + \Delta t) &= f_{(i)}(\mathbf{r}, t) + [(\partial_t + \partial_{(i)})f_{(i)}](\mathbf{r}, t)\Delta t \\ &\quad + [(\partial_t + \partial_{(i)})^2 f_{(i)}](\mathbf{r}, t)(\Delta t)^2/2 + \mathrm{O}(\Delta t)^3 \\ &= f_{(i)}(\mathbf{r}, t) + [\Delta t \partial'_{(i)} f_{(i)}](\mathbf{r}, t)\varepsilon + [(\Delta t \partial'_t \\ &\quad + (\Delta t \partial'_{(i)})^2/2) f_{(i)}](\mathbf{r}, t)\varepsilon^2 + \mathrm{O}(\varepsilon)^3 + \mathrm{O}(\Delta t)^3 \end{aligned} \tag{A.7}$$

and then applying $M_0[\cdot] = \sum_{i=0}^{K}(\cdot)$ to Eq. (21), leads upon use of (A.5) and (A.6) to

$$F_0 + F_1\varepsilon = Q_R/C + \mathrm{O}(\varepsilon)^2 \Delta t + \mathrm{O}(\varepsilon)^3/\Delta t + \mathrm{O}(\Delta t^2),$$
$$F_0 = \varepsilon^2 \partial'_t \sum_{i=0}^{K} f_{(i)} = \partial_t T, \quad F_1 = \sum_{i=0}^{K} \partial'_{(i)} f_{(i)}. \tag{A.8}$$

Since $M_1[q'] = (Q_R/C)M_1[f^{eq}] = 0$ in view of (A.5), the decomposition (A.4) leads to the estimate

$$\begin{aligned}\varepsilon F_1 &= \varepsilon\nabla'\cdot M_1[f^{eq} + f'_{(i)}\varepsilon + O(\varepsilon)^2]\\ &= \varepsilon\tau\nabla\cdot M_1[q'_{(i)} - \partial'_{(i)}f^{eq}_{(i)}] + \varepsilon\nabla'\cdot M_1[O(\varepsilon)^2]\\ &= -\tau\nabla\nabla : M_2[f^{eq}] + \nabla'\cdot M_1[O(\varepsilon)^3]\\ &= (-\nabla^2 T)\tau c_v/3 + O(\varepsilon)^3.\end{aligned}$$

Inserting now the results for F_0 and F_1 into the first equation in (A.8) yields

$$\begin{aligned}Q_R &= (F_0 + F_1\varepsilon) + (O(\Delta t)^2 + O(\varepsilon)^3/\Delta t + O(\varepsilon)^2\Delta t)\\ &= (\partial/\partial t - (\tau - \Delta t/2)c_v/3)T(\mathbf{r},t) + (O(\Delta t)^2\\ &\quad + O(\varepsilon)^3/\Delta t + O(\varepsilon)^2\Delta t). \qquad (A.9)\end{aligned}$$

The error term $O(\varepsilon)^3$ of εF_1 has been absorbed into $O(\varepsilon)^3/\Delta t$. The error terms in (A.9) are dominated either (i) by the $O(\varepsilon)^3/\Delta t$ term when $\varepsilon > O(\Delta t)$, or (ii) by an $O(\Delta t)^2$ contribution when $\Delta t \geqslant O(\varepsilon)$. One of the retained terms, F_0, was formally of $O(\varepsilon)^2$, so the option (i) must be excluded. For the remaining option (ii), an approximation to Eq. (3) of second order, i.e. with error terms of $O(\Delta t)^2$, can be obtained from (A.9) by requiring the relation (22) between diffusivity and relaxation parameter. Another implication of (ii) is, in view of the decomposition (A.4), that $|f_{(i)} - f^{eq}_{(i)}| \leqslant O(\Delta t)$.

Appendix B

The densities to be specified on the west boundary are $f_{(1)}$, $f_{(5)}$, and $f_{(8)}$. The case of $f_{(1)}$was considered in the main text. The other two follow in the same way, the overall result being

$$\begin{aligned}f_{(1)}(0,y,t) &= (2/9)T_0 - f_{(3)}(0,y,t),\\ f_{(5)}(0,y,t) &= (1/18)T_0 - f_{(7)}(0,y,t),\\ f_{(8)}(0,y,t) &= (1/18)T_0 - f_{(6)}(0,y,t).\end{aligned}$$

The unknowns on the east boundary are computed by "inverting" the above relations:

$$\begin{aligned}f_{(3)}(X,y,t) &= (2/9)T_0 - f_{(1)}(X,y,t),\\ f_{(6)}(X,y,t) &= (1/18)T_0 - f_{(8)}(X,y,t),\\ f_{(7)}(X,y,t) &= (1/18)T_0 - f_{(5)}(X,y,t).\end{aligned}$$

Similarly, on the north boundary,

$$\begin{aligned}f_{(4)}(x,Y,t) &= (2/9)T_0 - f_{(2)}(x,Y,t),\\ f_{(7)}(x,Y,t) &= (1/18)T_0 - f_{(5)}(x,Y,t),\\ f_{(8)}(x,Y,t) &= (1/18)T_0 - f_{(6)}(x,Y,t).\end{aligned}$$

On the sound boundary, the imposed value of the temperature is different:

$$\begin{aligned}f_{(2)}(x,0,t) &= (2/9)T_S - f_{(4)}(x,0,t),\\ f_{(5)}(x,0,t) &= (1/18)T_S - f_{(7)}(x,0,t),\\ f_{(6)}(x,0,t) &= (1/18)T_S - f_{(8)}(x,0,t).\end{aligned}$$

References

[1] S. Chen, G.D. Doolen, Lattice Boltzmann method for fluid flows, Annu. Rev. Fluid Mech. 30 (1998) 329–364.

[2] X. He, S. Chen, G.D. Doolen, A novel thermal model for the lattice Boltzmann method in the incompressible limit, J. Comput. Phys. 146 (1998) 282–300.

[3] B. Chopard, P.O. Luthi, Lattice Boltzmann computations and applications to physics, Theor. Comput. Phys. 217 (1999) 115–130.

[4] D.A. Wolf-Gladrow, Lattice Gas Cellular Automata and Lattice Boltzmann Models: An Introduction, Springer Verlag, Berlin–Heidelberg, 2000.

[5] R.G.M. von der Sman, M.H. Ernst, A.C. Berkerbosch, Lattice Boltzmann scheme for cooling of packed cut flowers, Int. J. Heat Mass Transfer 43 (2000) 577–587.

[6] J.-R. Ho, C.-P. Kuo, W.-S. Jiaung, C.-J. Twu, Lattice Boltzmann scheme for hyperbolic heat conduction equation, Int. J. Heat Mass Transfer, Part B 41 (2002) 591–607.

[7] J.-R. Ho, C.-P. Kuo, W.-S. Jiaung, Study of heat transfer in multilayered structure within the framework of dual-phase-lag heat conduction model using lattice Boltzmann method, Int. J. Heat Mass Transfer 46 (2003) 55–69.

[8] R.R. Nourgaliev, T.N. Dinh, T.G. Theofanous, D. Joseph, The lattice Boltzmann equation method: theoretical interpretation, numerics and implications, Int. J. Multiphase Flow 29 (2003) 117–169.

[9] S. Succi, The Lattice Boltzmann Equation for Fluid Dynamics and beyond, Oxford University Press, 2001.

[10] J.G.M. Eggels, J.A. Sommers, Numerical simulation of free convective flow using the lattice Boltzmann scheme, Int. J. Heat Fluid Flow 16 (1995) 357–364.

[11] W.-S. Jiaung, J.-R. Ho, C.-P. Kuo, Lattice Boltzmann scheme for hyperbolic heat conduction equation, Numer. Heat Transfer B 39 (2001) 167–187.

[12] X. Shan, Simulation of Rayleigh–Benard convection using a lattice Boltzmann method, Phys. Rev. E 55 (1997) 2780–2788.

[13] S.C. Mishra, A. Lankadasu, Transient conduction–radiation heat transfer in participating media using the lattice Boltzmann method and the discrete transfer method, Numer. Heat Transfer, Part A 47 (2005) 935–954.

[14] C.-Y. Wu, N.-R. Ou, Transient two-dimensional radiative and conductive heat transfer in a scattering medium, Int. J. Heat Mass Transfer 37 (1994) 2675–2686.

[15] W.W. Yuen, E.E. Takara, Analysis of combined conductive–radiative heat transfer in a two-dimensional rectangular enclosure with gray medium, J. Heat Transfer 110 (2) (1988) 468–474.

[16] T.Y. Kim, S.W. Baek, Analysis of combined conductive–radiative heat transfer in a two-dimensional rectangular enclosure using the discrete ordinate method, Int. J. Heat Mass Transfer 34 (9) (1991) 2265–2273.

[17] S.C. Mishra, P. Talukdar, D. Trimis, F. Durst, Computational efficiency improvements of the radiative transfer

problems with or without conduction—a comparison of the collapsed dimension method and the discrete transfer method, Int. J. Heat Mass Transfer 46 (16) (2003) 3083–3095.

[18] S.C. Mishra, M. Prasad, Radiative heat transfer in absorbing–emitting–scattering gray media inside 1-D Cartesian enclosure using the collapsed dimension method, Int. J. Heat Mass Transfer 45 (3) (2002) 697–700.

[19] P. Bhatnagar, E.P. Gross, M.K. Krook, A model for collision processes in gases I. Small amplitude processes in charged and neutral one-component systems, Phys. Rev. 94 (3) (1954) 511–525.